

ORIGINAL ARTICLE

Au/Ni₁₂P₅ core/shell nanocrystals from bimetallic heterostructures: *in situ* synthesis, evolution and supercapacitor properties

Sibin Duan¹ and Rongming Wang^{1,2}

A synthetic route to achieve core/shell nanostructures consisting of noble metal cores and single crystal semiconductor shells with different crystal systems is proposed, which involves a simple phosphorization process from corresponding bimetallic heterostructures. The triphenylphosphine is designed to serve as both a capping agent and a phosphorous source during the formation of Au/Ni₁₂P₅ core/shell nanoparticles (NPs) from Au-Ni bimetallic heterodimers. The semiconductor shells of the obtained Au/Ni₁₂P₅ nanostructures are controlled to form single crystals with a thickness of ~5 nm. The structure-dependent supercapacitor properties of Au-modified Ni₁₂P₅ nanostructures were further investigated. The synergistic effect of the metal/semiconductor nanostructure is observed to be superior to its oligomer-like counterpart when serving as a supercapacitor electrode. The specific capacitance of an electrode fabricated from core/shell NPs is 806.1 F g⁻¹ with a retention of 91.1% after 500 charge–discharge cycles.

NPG Asia Materials (2014) 6, e00; doi:10.1038/am.2014.65; published online 5 September 2014

INTRODUCTION

Noble metal–semiconductor heterostructures have attracted a substantial amount of interest for multi-functional applications in the areas of optoelectronics,^{1,2} catalysis,^{3–5} energy conversion^{6–8} and sensing⁹ because of their unique physical and chemical properties, which derive their benefits from synergistic effects. For example, Pt–CdSe–Pt nano-dumbbells exhibit an enhanced catalytic activity for CO oxidation when exposed to light radiation. This enhanced catalytic activity is attributed to the generation and transport of hot carriers along the interface of the Pt nanoparticles (NPs) and the CdSe semiconductor.¹⁰ Additionally, the Au–NiO nanohybrids exhibit significantly enhanced pseudo-capacitor properties due to the improved conductivity of the Au.¹¹ The synergistic effect of the heterostructures can be primarily attributed to the effect of interfaces.^{12–14} The core/shell nanostructure is regarded as one of the most promising heterostructures due to its controllable interface and surface.^{13,15–17} Specifically, the single crystalline semiconductor shell not only benefits the study of semiconductor physics at the nanoscale¹⁸ but also yields technological devices with optimum characteristics.^{19,20}

Various methods have been developed to synthesize metal–semiconductor core/shell nanostructures.^{12,21,22} Among these, the most widely used strategies rely on the so-called ‘seeded growth’ method, whereby the closely matched lattice parameters of core and shell components are crucial for obtaining a single crystalline shell.²³

In most cases, the undesired crystalline defects in the semiconductor shell are associated with weakened material properties and degraded device performance.^{24,25} The synthesis of core/shell nanostructures with substantial lattice mismatches, which cannot be obtained using the conventional seeded growth method, remains challenging. Only a few reports have been published on this subject, and these are still somewhat limited.^{22,26–29}

Here, we report a new synthetic method for obtaining core/shell nanostructures with single crystal semiconductor shells, which involves a simple phosphorization process from corresponding bimetallic heterostructures. The Ni₁₂P₅ semiconductor shells in the heterostructures are the promising candidates as the traditional fossil fuel purificant, energy resources, etc. Oligomer-like Au–Ni₁₂P₅ NPs were also synthesized using the traditional seeded growth method for comparison. The growth mechanism and structure-dependent electrochemical capacitor performances of the as-prepared nanostructures were also investigated in detail.

EXPERIMENTAL PROCEDURES

Chemicals

Nickel(II) acetylacetonate (Ni(acac)₂, 97.0%), chloroauric acid (HAuCl₄·4H₂O), oleylamine (OAm, 98.0%), triphenylphosphine (TPP, 99.0%), acetone (99.5%), chloroform (99.0%) and toluene (99.5%) were purchased from Sinopharm Chemical Reagent Beijing Co., Ltd. (Beijing, China). All reagents were analytic grade and used as-received without further purification.

¹Department of Physics, Beihang University, Beijing, P. R. China and ²Department of Physics, School of Mathematics and Physics, University of Science and Technology Beijing, Beijing, P. R. China

Correspondence: Professor R Wang, Department of Physics, Beihang University, Beijing 100191, P. R. China.

E-mail: rmwang@buaa.edu.cn or rmwang@ustb.edu.cn

Received 1 January 2014; revised 22 April 2014; accepted 2 June 2014

Synthesis of the Ni₁₂P₅ NPs

Ni(acac)₂ (0.5 g) was dissolved in 10 ml OAm before being heated to 100 °C for 15 min. Subsequently, TPP (1.0 g) was added to the blue-green solution and magnetically stirred for 30 min. The mixed solution was then heated to 270 °C for 60 min before being naturally cooled to room temperature. Finally, the product was collected by centrifugation, washed several times with acetone and resolved in toluene.

Synthesis of the Au–Ni heterodimer NPs

Ni(acac)₂ (0.5 g) was dissolved in 10 ml OAm before being heated to 100 °C for 15 min to form a blue-green solution. Subsequently, a freshly prepared solution of HAuCl₄ · 4H₂O (0.05 g in 5 ml of toluene) was added dropwise with stirring while maintaining a temperature of 100 °C for 60 min. The resulting dark purple solution was then heated to 230 °C for 60 min before being cooled to room temperature. Finally, the product was collected by centrifugation, washed several times with acetone and resolved in toluene.

Synthesis of the Au/Ni₁₂P₅ core/shell NPs

The synthesis of Au/Ni₁₂P₅ was based on the synthesis of Au–Ni heterodimer NPs. After the Au–Ni heterodimer NPs formed at 230 °C, TPP (1.0 g) was added and stirred for 30 min. Then, the mixed solution was heated to 270 °C for 60 min before being naturally cooled to room temperature. Finally, the product was collected by centrifugation, washed several times with acetone and resolved in toluene.

Synthesis of the Au–Ni₁₂P₅ oligomer-like NPs

As-prepared Ni₁₂P₅ NPs (0.44 g) were washed in 5 ml chloroform three times and dispersed in 10 ml OAm. The mixture was then heated to 230 °C for 30 min. Afterwards, a freshly prepared solution of HAuCl₄ · 4H₂O (0.05 g in 5 ml of toluene) was added while stirring and kept at 230 °C for 15 min. After naturally cooling to room temperature, the product was collected by centrifugation, washed several times with acetone and resolved in toluene.

Materials characterization

The crystal structures, morphologies and chemical compositions of the as-prepared products were studied using X-ray diffraction (XRD, Rigaku Dmax2200, Cu K α , Tokyo, Japan) and transmission electron microscopy (TEM, JEOL 2100F (Tokyo, Japan) with a field emission gun and an accelerating voltage of 200 kV). For the XRD measurements, powder samples dried in a vacuum drying oven were used. The specimen used for the TEM investigation was prepared by dispersing a drop of solution onto a porous carbon film supported on a copper grid, and it was dried in vacuum drying oven.

Electrochemical measurements

The electrochemical measurements were carried out in a three-electrode electrochemical cell containing 2 M KOH aqueous solution as electrolyte. The working electrode was prepared by mixing the electroactive material, carbon black (with a measured specific capacitance of 7.5, 6.6, 5.6, 4.1, 2.6 and 1.3 F g⁻¹ at current densities of 0.2, 0.3, 0.5, 1, 2 and 5 A g⁻¹, respectively) and polytetrafluoroethylene at a weight ratio of 7:2:1. The mixture was dispersed into acetone for homogeneity and then pressed on the Ni foam (1 cm²) as the working electrode and dried at 60 °C for 24 h in a vacuum drying oven. Cyclic voltammetry and chronopotentiometry were performed on a CHI660E electrochemical workstation (Chenhua, Shanghai). The Hg/HgO electrode and the Ni foam electrode were used as the reference and the counter electrodes, respectively. Electrochemical impedance spectrum measurements were carried out using this apparatus over a frequency spectrum range of 100 kHz to 0.01 Hz at 0 V with an AC amplitude of 5 mV.

RESULTS AND DISCUSSION

Morphological and structural characterization

The as-synthesized materials were first identified as Au/Ni₁₂P₅ NPs with a core/shell nanostructure. From the low-magnification TEM image shown in Figure 1a, the darker cores and the brighter shells clearly suggest the formation of a core/shell structure with a core

diameter of ~5 nm. Additionally, these NPs exhibit a truncated-octahedron morphology with a length of ~16–20 nm. The as-prepared NPs are homogeneously dispersed with high uniformity. Figure 1c shows the powder XRD pattern of the product. From this image, the diffraction peaks of face-centered cubic (f.c.c.) Au phase (JCPDF No. 04-0784) and body-centered tetragonal (b.c.t.) Ni₁₂P₅ phase (JCPDF No. 74-1381) can be clearly observed. Broadening of the XRD peaks may result from the small grain sizes, which are estimated to be ~14 nm for the Au using the (111) peak and ~22 nm for the Ni₁₂P₅ using the (312) peak by Scherrer's equation $d = 0.89\lambda / (\beta \cdot \cos\theta_B)$, where λ is the X-ray wavelength (0.15406 nm), θ_B is the Bragg diffraction angle and β is the peak full width at half-maximum. The energy dispersive X-ray spectroscopy (EDS) results are shown in Supplementary Figure S1. The atomic ratio of Au/Ni is calculated to be 8:92, and the atomic ratio of Ni/P is 2.23. This Ni/P ratio is less than the stoichiometric ratio for Ni₁₂P₅ (2.4), which is most likely a result of the TPP coated on the NP surfaces.

To investigate the nanostructure in greater detail, high-resolution transmission electron microscopy (HRTEM) characterization was conducted. The HRTEM image in Figure 1b clearly shows the single crystal nature of the Ni₁₂P₅ shell. The lattice spacing measured from the core and the shell is 0.237 and 0.194 nm, corresponding to the f.c.c. Au (111) planes and the b.c.t. Ni₁₂P₅ (240) planes, respectively. The good crystallinity of the as-grown Ni₁₂P₅ shells is additionally revealed by angle-dependent TEM characterization using various viewing angles (Supplementary Figure S2), further verifying the core/shell structure of the products. In addition, the EDS mapping spectrum for an individual NP is shown in Figure 1d, which denotes the elemental distribution of Au, Ni and P in the NP. All the results confirm the formation of core/shell Au/Ni₁₂P₅ NPs with single crystal semiconductor shells.

Growth mechanism

Because of the large lattice mismatch between the Au and the Ni₁₂P₅, it is difficult to form a perfect core/shell nanostructure, especially with a single crystal shell. Understanding the growth mechanism is critically important and can provide more insight into a new synthesis method for other types of noble metal-modified semiconductor nanomaterials.

From heterodimer Au–Ni NPs to core/shell Au/Ni₁₂P₅ NPs

Time-dependent experiments were first conducted to investigate the growth mechanism in-depth. As shown in Figure 2, after adding TPP into the OAm containing the Au–Ni heterodimer NPs (a detailed characterization is shown in Supplementary Figure S3) and raising the system temperature from 230 to 270 °C, the morphology of the NPs changes from the dumbbell-like heterodimer to a core/shell structure containing Au coated by Ni₁₂P₅. Meanwhile, the octahedral shape becomes more distinct as reaction time elapses. It is noted that the size and shape of Au NPs do not obviously change during this process. As shown in Supplementary Figure S4, the atomic ratio of Ni to P obtained from the EDS results at different times decreases from 5.6 at 5 min to 2.23 at 60 min after adding TPP, indicating the gradual phosphorization process of Ni to form nickel phosphide. Herein, during the component and morphology transformation process, two important factors, the synthesis temperature and the addition of TPP are highlighted. To disclose their effects on the formation of Au/Ni₁₂P₅ NPs, a number of comprehensive experiments were conducted.

When the temperature was maintained at 230 °C and for the same amount of additional TPP added into the OAm containing Au–Ni

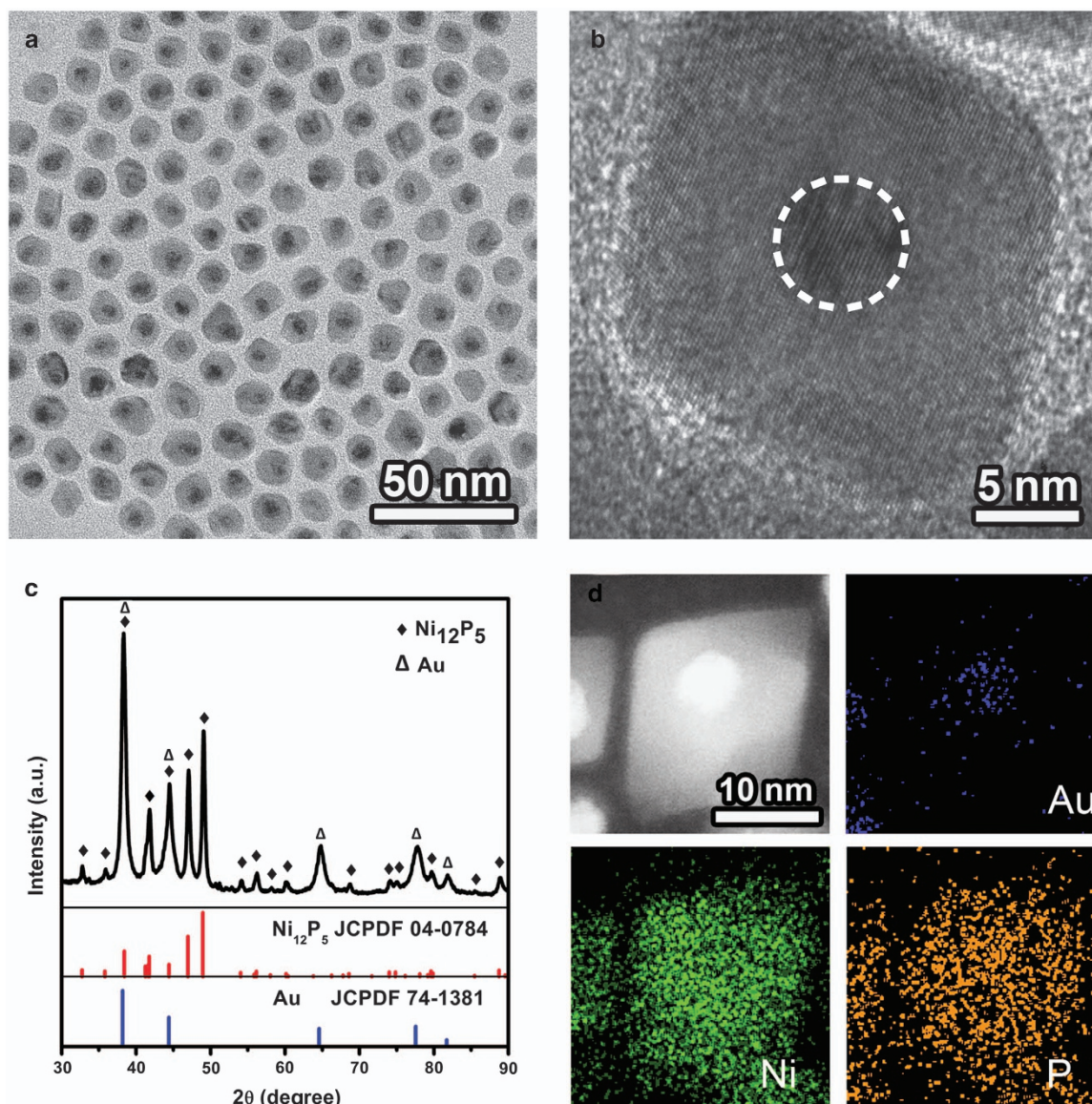


Figure 1 Au/Ni₁₂P₅ core/shell NPs: (a) an overview TEM image showing the core/shell nanostructure; (b) HRTEM image of a single NP; (c) XRD pattern of the as-synthesized Au/Ni₁₂P₅ NPs indexed to f.c.c. Au and b.c.t. Ni₁₂P₅; and (d) EDS element mapping of one representative Au/Ni₁₂P₅ NP.

heterodimer NPs, the NPs remained as dumbbell-like heterodimers without any obvious changes in morphology, and the lattice distances measured from the HRTEM image were indexed to f.c.c. Au (111) and f.c.c. Ni (111), confirming that the product is still Au–Ni bimetallic NPs (Supplementary Figure S5a and b). From the EDS spectrum, no obvious P signal can be observed within the detection limit, indicating that there are no nickel phosphides present, which agrees with the XRD results (Supplementary Figure S5c and d). This evidence indicates that the phosphorization process of Ni in an OAm system requires a relatively higher temperature—270 °C—in this work, which is slightly lower than that reported in other work.^{30,31} It also indicates that the heterodimer Au–Ni NPs are relatively stable at 230 °C.

Many reports have indicated that the formation of nanoscale hetero-interfaces in a solution phase can be greatly influenced by the binding of organic stabilizers, which can significantly impact on the surface energy terms and, consequently, alter the ultimate Gibbs free

energy balance.^{23,27} To investigate the effect of TPP on the evolution of Au–Ni bimetallic heterodimers to Au/Ni₁₂P₅ core/shell nanostructures, the solution temperature of OAm containing Au–Ni heterodimer NPs was increased to 270 °C without the addition of any TPP. The Au–Ni NPs did not retain their dumbbell-like morphology, whereas polyhedron AuNi segregated NPs can be observed, as shown in Supplementary Figure S6. Such a recrystallization process is accompanied by the migration of Ni and Au atoms, which has been previously investigated *in situ* using scanning transmission electron microscopy.³² From the experimental results, we can conclude that TPP is an effective capping agent for Au atoms in the Ni phosphorization process. TPP can tightly bind to the surface atoms of Au NPs, preventing the Au atoms from migrating and favoring the formation of a gold core in the final Au/Ni₁₂P₅ NPs. To verify the capping effect of the TPP for Au, we replaced TPP with trioctyl phosphate (TOP). Interestingly, no any form of nickel phosphides formed, even when the temperature was raised as high as 320 °C.

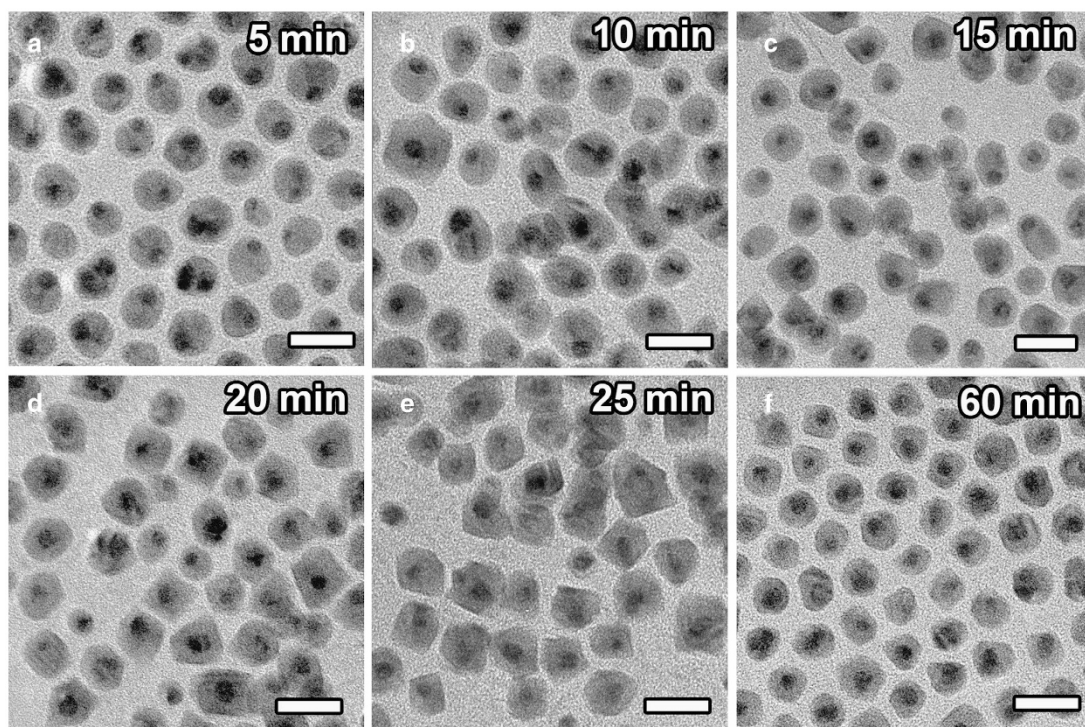


Figure 2 TEM images of the product at different times after adding TPP, indicating that the final core/shell Au/Ni₁₂P₅ NPs are converted from heterodimer Au–Ni NPs. Scale bar: 20 nm.

As shown in Supplementary Figure S7, eutectic Au–Ni bimetallic NPs were obtained. Similar to the product obtained from the experiment performed without the addition of TPP, the EDS and XRD results reveal that the products are AuNi bimetallic NPs. We can therefore deduce that the capping effect of TOP on Au atoms is not as strong as TPP because of the lack of unshared electrons in the P atoms in the TOP, which because of P=O bonding. Thus, it is possible to allow the Au atoms access to the surrounding medium.

Furthermore, when TPP is added into the synthesis system of Au NPs in OAm, no Au NP is obtained. Comparatively, the icosahedron Au NPs were obtained with TOP, which again verifies the TPP capping effect.

Therefore, the TPP can serve as both the phosphorus source in the phosphorization process and the capping agent on the Au surface, which is crucial for the formation of the core/shell structure. The evolution process from Au–Ni heterodimers to the core/shell Au/Ni₁₂P₅ NPs can be described as follows: (1) the Au components in the Au–Ni NPs are coated with TPP on their surfaces, which prevents the Au from migrating, forming the core finally; (2) the TPP serves as an effective phosphorus source for the Ni part of the Au–Ni NPs, and convert the Ni into Ni₁₂P₅ gradually; and (3) the Ni components migrate and recrystallize into the single crystalline Ni₁₂P₅ shell accompanying the phosphorization process at elevated temperatures. Following this procedure, Au–Ni heterodimer NPs are gradually converted into core/shell Au/Ni₁₂P₅ NPs. The transformation process is illustrated in Figure 3.

Electrochemical properties of noble metal-modified Ni₁₂P₅ NPs

Supercapacitors are a type of energy storage device that have attracted significant interest in recent years due to their high power density, good cycling performance, rapid charge/discharge characteristics and environmentally friendly nature.^{33,34} In particular, nickel phosphides

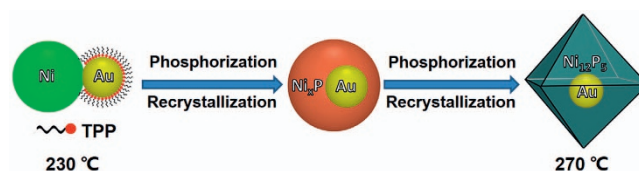


Figure 3 Schematic illustration of the formation of the Au/Ni₁₂P₅ core/shell NPs.

are promising pseudo-capacitor materials.^{35,36} Here, we investigate and compare the performances of supercapacitors composed of as-prepared gold-modified Ni₁₂P₅ NPs and pure Ni₁₂P₅ NPs in a 2 M KOH aqueous solution. Supplementary Figure S12a, c and e presents typical cyclic voltammograms of pure Ni₁₂P₅, core/shell Au/Ni₁₂P₅ and oligomer-like Au–Ni₁₂P₅ NPs at different scan rates, respectively. The characterizations of the pure Ni₁₂P₅, oligomer-like Au–Ni₁₂P₅ and separated Au&Ni₁₂P₅ are shown in Supplementary Figures S8, S9 and S10, respectively. The summary of the formation of Au-modified Ni₁₂P₅ and pure Ni₁₂P₅ NPs with different nanostructures is shown in Supplementary Figure S11. Two strong redox peaks are observed in every curve, indicating the capacitance characteristics are mainly pseudo-capacitive capacitances due to Faradaic redox reactions.

To further evaluate the electrochemical properties and estimate the capacity of the three different types of NPs, galvanostatic charging and discharging of the pure Ni₁₂P₅, core/shell Au/Ni₁₂P₅ and oligomer-like Au–Ni₁₂P₅ NPs in a 2 M KOH solution was performed. Figure 4a–c shows the galvanostatic discharge curves of the pure Ni₁₂P₅, core/shell Au/Ni₁₂P₅ and oligomer-like Au–Ni₁₂P₅ electrodes at different current rates, respectively. The specific capacitance of the electrode can be calculated from the discharge curve according to

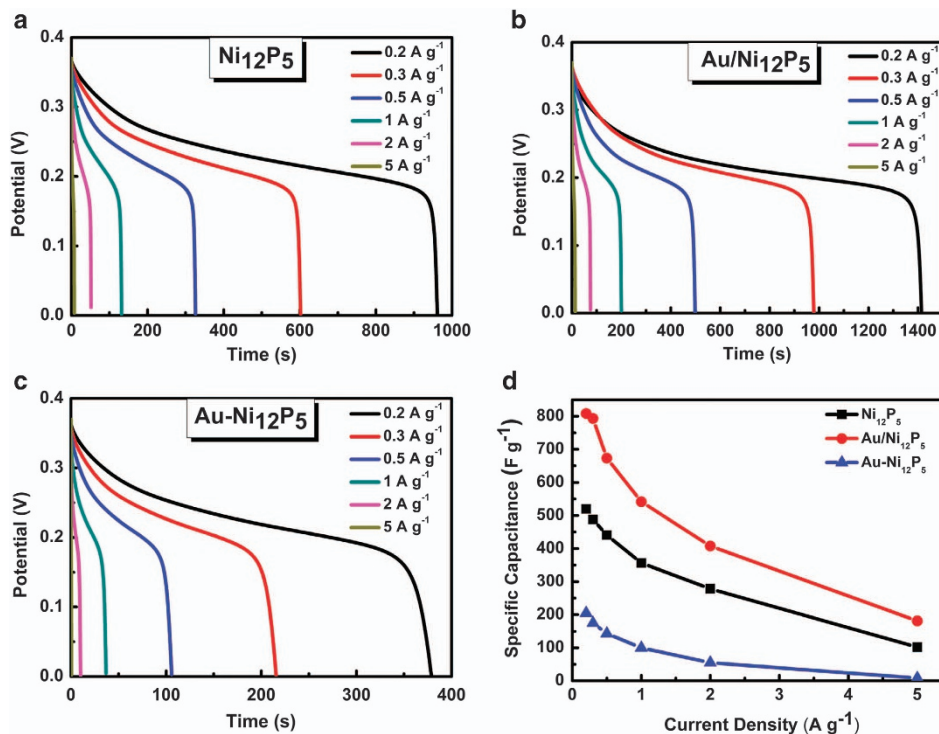


Figure 4 Discharge voltage profiles at different current densities for (a) pure Ni₁₂P₅ NPs, (b) core/shell Au/Ni₁₂P₅ NPs, (c) oligomer-like Au-Ni₁₂P₅ NPs and (d) specific capacitances derived from the discharge curves.

Equation 1:

$$C = \frac{I\Delta t}{m\Delta V}, \quad (1)$$

where C (F g⁻¹) is the specific capacitance, I (mA) is the discharge current, Δt (s) is the discharge time, m (g) is the mass of the active material in the electrode and ΔV (V) is the potential change during the discharge. The specific capacitances derived from the discharge curves are shown in Figure 4d. From the calculated results, it is evident that the core/shell Au/Ni₁₂P₅ NPs possess the highest specific capacitance, whereas the electrode made of oligomer-like Au-Ni₁₂P₅ NPs is the poorest performer of the three types of Ni₁₂P₅-based nanomaterials investigated here. At a current density of 0.2 A g⁻¹, the specific capacitances of the pure Ni₁₂P₅, the core/shell Au/Ni₁₂P₅ and the oligomer-like Au-Ni₁₂P₅ NPs are 517.4, 806.1 and 202.6 F g⁻¹, respectively. The normalized specific capacitances of the core/shell Au/Ni₁₂P₅ and the oligomer-like Au-Ni₁₂P₅ NPs determined by subtracting the gold content from the electrodes are 1007.8 and 313.2 F g⁻¹, respectively. The masses of the gold in the as-prepared NPs are calculated from the EDS results, which agree with the ratio of the initial precursors. This demonstrates that the specific capacitance of the Au/Ni₁₂P₅ core/shell NPs is clearly enhanced by 94.8% compared with the pure Ni₁₂P₅. However, the gold component does not enhance the supercapacitor properties of nickel phosphide in the oligomer-like Au-Ni₁₂P₅ NPs. Therefore, a synergistic effect exists between the Au components and the Ni₁₂P₅ components through the formation of the Au/Ni₁₂P₅ core/shell structures.

Good specific capacitance retention is also important for electrode materials. Here, the cyclic stability of the pure Ni₁₂P₅, the core/shell Au/Ni₁₂P₅ and the oligomer-like Au-Ni₁₂P₅ electrodes are investigated at a current density of 1 A g⁻¹. After 500 charge/discharge cycles, the specific capacitances for the electrodes fabricated from the pure

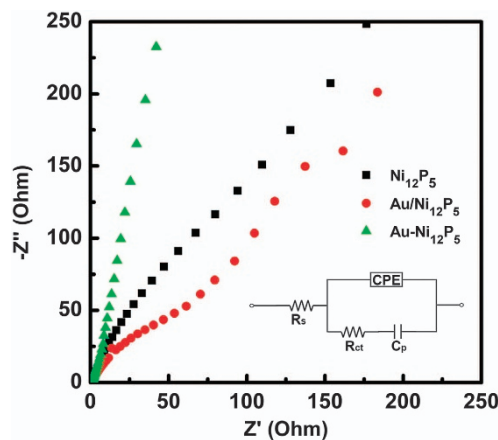


Figure 5 Nyquist plots of the pure Ni₁₂P₅ (black), core/shell Au/Ni₁₂P₅ (red) and oligomer-like Au-Ni₁₂P₅ (green) electrodes. The inset shows the equivalent circuit diagram.

Ni₁₂P₅, the core/shell Au/Ni₁₂P₅ and the oligomer-like Au-Ni₁₂P₅ NPs decrease to 300.3, 492.3 and 74.2 F g⁻¹, respectively (see Supplementary Figure S12). Similar to the results for the specific capacitance, the core/shell Au/Ni₁₂P₅ exhibits the best cyclic stability, maintaining 91.1% stability after 500 cycles. Similar to the previous results, the oligomer-like Au-Ni₁₂P₅ NPs only maintain 75.3% stability after 500 cycles, which is the lowest of the three electrodes investigated here.

These results demonstrate that the NPs with core/shell structure obtain both the best cyclic stability and the highest specific capacitance among the three Ni₁₂P₅-based electrodes. To identify the exact electrical conductivity of the three electrodes, electro-

chemical impedance spectrums were measured at room temperature over a frequency range from 100 kHz to 0.01 Hz under open-circuit conditions. As shown in Figure 5, the Nyquist plots for the three electrodes show two partially overlapping semicircles in the high- and medium-frequency regions and an inclined line in the low-frequency region. The equivalent circuit used to fit the impedance curve is given in the insert of Figure 5. The electrochemical impedance spectral data can be fitted by a bulk system resistance R_s , a charge-transfer resistance R_{ct} , a pseudo-capacitance element C_p from the redox process, and a CPE that accounts for the double-layer capacitance. The charge-transfer resistance (R_{ct}) is the decisive parameter for the three supercapacitor electrodes.^{37,38} Using the ZSimpWin software (Princeton Applied Research, Oak Ridge, TN, USA), the charge-transfer resistance R_{ct} of the Ni₁₂P₅, Au/Ni₁₂P₅ and Au–Ni₁₂P₅ electrodes are calculated to be 184.7, 0.18 and 31.75 Ω, respectively. The core/shell Au/Ni₁₂P₅ has the lowest charge-transfer resistance of the three samples by 2–3 orders of magnitude. This can be attributed to the enhanced electric conductivity and/or short charge diffusion lengths due to the synergistic effect between the metallic cores and the semiconductor shells, or the strong interfacial electronic coupling and/or the enhanced spin-orbit coupling in metals and semiconductors at the nanoscale.^{18,37,38} Consequently, easy transport paths for the ions (electrolytes) associated with high charge density can be formed, leading to the highest specific power in the Au/Ni₁₂P₅ electrode. The thin single crystalline shell also benefits much for good ionic diffusion and electron transport. As for the Au–Ni₁₂P₅ electrode, even though the charge-transfer resistance (R_{ct}) is lower than that of the pure Ni₁₂P₅ electrode, its supercapacitor properties were the lowest. This result is due to the distinct microstructural differences between the Au/Ni₁₂P₅ core/shell NPs and the oligomer-like Au–Ni₁₂P₅ NPs. Although the gold components attached to the outer surface of the Ni₁₂P₅ favor reduction in R_{ct} , these gold components can also foster charge transport from the Ni₁₂P₅ to the electrolytes, leading to a reduced charge density and stability in the Ni₁₂P₅ that is contrary to the role of the Au components in the core of the Ni₁₂P₅ NPs. In addition, due to the large specific surface area (Supplementary Table S1) and high surface energy, a homogeneous dispersion among the Au–Ni₁₂P₅ NPs and carbon black is difficult to achieve. Thus, only a small number of NPs can directly come into contact with the carbon additive and store electrons, leading to a small specific capacitance, as reported in other work.³⁹ Therefore, comprehensively, the oligomer-like Au–Ni₁₂P₅ NPs have the lowest specific capacitance.

CONCLUSION

In summary, we have synthesized noble metal-modified nickel phosphide NPs with core/shell heterostructures. The synthesis method of converting pre-formed Au–Ni heterodimers into core/shell Au/Ni₁₂P₅ NPs has proven to be a simple and efficient route to fabricate noble metal-modified semiconductor nanomaterials. Until now, much progress has been achieved in the synthesis of bimetallic NPs with different components and morphologies, which provides us with a wide range of starting materials to yield corresponding metal-modified semiconductor NPs.⁴⁰ The synthesis methodology proposed in this paper defines a new way to obtain metal–semiconductor hetero-structures with a perfect crystalline nature. Furthermore, the results from the electrochemical property experiments on the as-prepared noble metal-modified Ni₁₂P₅ NPs indicate that the core/shell Au/Ni₁₂P₅ NPs exhibit the best supercapacitor properties, with a specific capacitance of up to 806.1 F g^{−1} that can be maintained at 91.1% after 500 charge–discharge cycles. It is believed that the noble

metal-modified metal phosphides will open up new opportunities for metal phosphides in a broader range of applications, such as energy storage materials, lithium ion batteries or hydrodesulfurization catalysts.

ACKNOWLEDGEMENTS

This work was supported by the National Natural Science Foundation of China (Nos. 11174023, 51371015 and 51331002), the Beijing Municipal Research Project for Outstanding Doctoral Thesis Supervisors (No. 20121000603), the Beijing Natural Science Foundation (No. 2142018) and the Fundamental Research Funds for the Central Universities.

- 1 Talapin, D. V., Lee, J. S., Kovalenko, M. V. & Shevchenko, E. V. Prospects of colloidal nanocrystals for electronic and optoelectronic applications. *Chem. Rev.* **110**, 389–458 (2010).
- 2 Pu, Y. C., Wang, G., Chang, K. D., Ling, Y., Lin, Y. K., Fitzmorris, B. C., Liu, C. M., Lu, X., Tong, Y., Zhang, J. Z., Hsu, Y. J. & Li, Y. Au nanostructure-decorated TiO₂ nanowires exhibiting photoactivity across entire UV-visible region for photoelectrochemical water splitting. *Nano Lett.* **13**, 3817–3823 (2013).
- 3 Qu, Y. & Duan, X. Progress, challenge and perspective of heterogeneous photocatalysts. *Chem. Soc. Rev.* **42**, 2568–2580 (2013).
- 4 Yang, J., Wang, D., Han, H. & Li, C. Roles of cocatalysts in photocatalysis and photoelectrocatalysis. *Acc. Chem. Res.* **46**, 1900–1909 (2013).
- 5 Rawalekar, S. & Mokari, T. Rational design of hybrid nanostructures for advanced photocatalysis. *Adv. Energy Mater.* **3**, 12–27 (2013).
- 6 Lincic, S., Christopher, P. & Ingram, D. B. Plasmonic-metal nanostructures for efficient conversion of solar to chemical energy. *Nat. Mater.* **10**, 911–921 (2011).
- 7 McFarland, E. W. & Tang, J. A photovoltaic device structure based on internal electron emission. *Nature* **421**, 616–618 (2003).
- 8 Oldfield, G., Ung, T. & Mulvaney, P. Au@SnO₂ core-shell nanocapacitors. *Adv. Mater.* **12**, 1519–1522 (2000).
- 9 Wang, H., Sun, Z., Lu, Q., Zeng, F. & Su, D. One-pot synthesis of (Au nanorod)-(metal sulfide) core-shell nanostructures with enhanced gas-sensing property. *Small* **8**, 1167–1172, 1124 (2012).
- 10 Kim, S. M., Lee, S. J., Kim, S. H., Kwon, S., Yee, K. J., Song, H., Somorjai, G. A. & Park, J. Y. Hot carrier-driven catalytic reactions on Pt–CdSe–Pt nanodumbbells and Pt/GaN under light irradiation. *Nano Lett.* **13**, 1352–1358 (2013).
- 11 Qu, B., Hu, L., Chen, Y., Li, C., Li, Q., Wang, Y., Wei, W., Chen, L. & Wang, T. Rational design of Au–NiO hierarchical structures with enhanced rate performance for supercapacitors. *J. Mater. Chem. A* **1**, 7023 (2013).
- 12 Buck, M. R. & Schaak, R. E. Emerging strategies for the total synthesis of inorganic nanostructures. *Angew. Chem. Int. Ed. Engl.* **52**, 6154–6178 (2013).
- 13 Lee, J. S., Shevchenko, E. V. & Talapin, D. V. Au–PbS core-shell nanocrystals: plasmonic absorption enhancement and electrical doping via intra-particle charge transfer. *J. Am. Chem. Soc.* **130**, 9673–9675 (2008).
- 14 Kochuveedu, S. T., Jang, Y. H. & Kim, D. H. A study on the mechanism for the interaction of light with noble metal-metal oxide semiconductor nanostructures for various photophysical applications. *Chem. Soc. Rev.* **42**, 8467–8493 (2013).
- 15 Wei, S., Wang, Q., Zhu, J., Sun, L., Lin, H. & Guo, Z. Multifunctional composite core-shell nanoparticles. *Nanoscale* **3**, 4474–4502 (2011).
- 16 Song, Y., Ding, J. & Wang, Y. Shell-dependent evolution of optical and magnetic properties of Co@Au core-shell nanoparticles. *J. Phys. Chem. C* **116**, 11343–11350 (2012).
- 17 Duan, S. B. & Wang, R. M. Bimetallic nanostructures with magnetic and noble metals and their physicochemical applications. *Prog. Nat. Sci. Mater.* **23**, 113–126 (2013).
- 18 Boross, P., Dora, B., Kiss, A. & Simon, F. A unified theory of spin-relaxation due to spin-orbit coupling in metals and semiconductors. *Sci. Rep.* **3**, 3233 (2013).
- 19 Battaglia, D., Li, J. J., Wang, Y. & Peng, X. Colloidal two-dimensional systems: CdSe quantum shells and wells. *Angew. Chem. Int. Ed. Engl.* **42**, 5035–5039 (2003).
- 20 Klimov, V. I., Ivanov, S. A., Nanda, J., Achermann, M., Bezel, I., McGuire, J. A. & Piryatinski, A. Single-exciton optical gain in semiconductor nanocrystals. *Nature* **447**, 441–446 (2007).
- 21 Feng, X., Hu, G. & Hu, J. Solution-phase synthesis of metal and/or semiconductor homojunction/heterojunction nanomaterials. *Nanoscale* **3**, 2099–2117 (2011).
- 22 Zhang, J., Tang, Y., Weng, L. & Ouyang, M. Versatile strategy for precisely tailored core@shell nanostructures with single shell layer accuracy: the case of metallic shell. *Nano Lett.* **9**, 4061–4065 (2009).
- 23 Carbone, L. & Cozzoli, P. D. Colloidal heterostructured nanocrystals: Synthesis and growth mechanisms. *Nano Today* **5**, 449–493 (2010).
- 24 McBride, J., Treadway, J., Feldman, L. C., Pennycook, S. J. & Rosenthal, S. J. Structural basis for near unity quantum yield core/shell nanostructures. *Nano Lett.* **6**, 1496–1501 (2006).
- 25 Chen, X. B., Lou, Y. B., Samia, A. C. & Burda, C. Coherency strain effects on the optical response of core/shell heteronanostructures. *Nano Lett.* **3**, 799–803 (2003).
- 26 Zhang, J., Tang, Y., Lee, K. & Ouyang, M. Tailoring light-matter-spin interactions in colloidal hetero-nanostructures. *Nature* **466**, 91–95 (2010).

- 27 Zhang, J., Tang, Y., Lee, K. & Ouyang, M. Nonepitaxial growth of hybrid core-shell nanostructures with large lattice mismatches. *Science* **327**, 1634–1638 (2010).
- 28 Zanella, M., Falqui, A., Kudera, S., Manna, L., Casula, M. F. & Parak, W. J. Growth of colloidal nanoparticles of group. II–VI and IV–VI semiconductors on top of magnetic iron–platinum nanocrystals. *J. Mater. Chem.* **18**, 4311 (2008).
- 29 Gao, J., Zhang, B., Gao, Y., Pan, Y., Zhang, X. & Xu, B. Fluorescent magnetic nanocrystals by sequential addition of reagents in a one-pot reaction: a simple preparation for multifunctional nanostructures. *J. Am. Chem. Soc.* **129**, 11928–11935 (2007).
- 30 Chiang, R. K. & Chiang, R. T. Formation of hollow Ni₂P nanoparticles based on the nanoscale Kirkendall effect. *Inorg. Chem.* **46**, 369–371 (2007).
- 31 Muthuswamy, E., Savithra, G. H. & Brock, S. L. Synthetic levers enabling independent control of phase, size, and morphology in nickel phosphide nanoparticles. *ACS Nano* **5**, 2402–2411 (2011).
- 32 Liu, W., Sun, K. & Wang, R. In situ atom-resolved tracing of element diffusion in NiAu nanospindles. *Nanoscale* **5**, 5067–5072 (2013).
- 33 Chen, L. F., Huang, Z. H., Liang, H. W., Guan, Q. F. & Yu, S. H. Bacterial-cellulose-derived carbon nanofiber@MnO₂ and nitrogen-doped carbon nanofiber electrode materials: an asymmetric supercapacitor with high energy and power density. *Adv. Mater.* **25**, 4746–4752 (2013).
- 34 Zhou, D., Su, X., Boese, M., Wang, R. & Zhang, H. Ni(OH)₂@Co(OH)₂ hollow nanohexagons: controllable synthesis, facet-selected competitive growth and capacitance property. *Nano Energy* **5**, 52–59 (2014).
- 35 Lu, Y., Liu, J. K., Liu, X. Y., Huang, S., Wang, T. Q., Wang, X. L., Gu, C. D., Tu, J. P. & Mao, S. X. Facile synthesis of Ni-coated Ni₂P for supercapacitor applications. *CrystEngComm* **15**, 7071–7079 (2013).
- 36 An, C. H., Wang, Y. J., Wang, Y. P., Liu, G., Li, L., Qiu, F. Y., Xu, Y. A., Jiao, L. F. & Yuan, H. T. Facile synthesis and superior supercapacitor performances of Ni₂P/rGO nanoparticles. *RSC Adv.* **3**, 4628–4633 (2013).
- 37 Lang, X., Hirata, A., Fujita, T. & Chen, M. Nanoporous metal/oxide hybrid electrodes for electrochemical supercapacitors. *Nat. Nanotechnol.* **6**, 232–236 (2011).
- 38 Pang, H., Wang, S., Li, G., Ma, Y., Li, J., Li, X., Zhang, L., Zhang, J. & Zheng, H. Cu superstructures fabricated using tree leaves and Cu–MnO₂ superstructures for high performance supercapacitors. *J. Mater. Chem. A* **1**, 5053 (2013).
- 39 Pang, H., Wei, C., Li, X., Li, G., Ma, Y., Li, S., Chen, J. & Zhang, J. Microwave-assisted synthesis of NiS₂ nanostructures for supercapacitors and cocatalytic enhancing photocatalytic H₂ production. *Sci. Rep.* **4**, 3577 (2014).
- 40 Duan, S. & Wang, R. Bimetallic nanostructures with magnetic and noble metals and their physicochemical applications. *Prog. Nat. Sci.* **23**, 113–126 (2013).



This work is licensed under a Creative Commons Attribution-NonCommercial-ShareAlike 3.0 Unported License. The images or other third party material in this article are included in the article's Creative Commons license, unless indicated otherwise in the credit line; if the material is not included under the Creative Commons license, users will need to obtain permission from the license holder to reproduce the material. To view a copy of this license, visit <http://creativecommons.org/licenses/by-nc-sa/3.0/>

Supplementary Information accompanies the paper on the NPG Asia Materials website (<http://www.nature.com/am>)

ERRATUM

Au/Ni₁₂P₅ core/shell nanocrystals from bimetallic heterostructures: *in situ* synthesis, evolution and supercapacitor properties

Sibin Duan and Rongming Wang

NPG Asia Materials (2015) 7, e172; doi:10.1038/am.2015.25; published online 10 April 2015

Correction to: *NPG Asia Materials* (2014) 6, e122; doi:10.1038/am.2014.65; published online 5 September 2014

The publisher would like to apologize for any inconvenience this may have caused.

The 'e' number was incorrect in the PDF version. It should be e122 instead of e00.

The correct citation to this article should be read as below:

NPG Asia Materials (2014) 6, e122; doi:10.1038/am.2014.65; published online 5 September 2014